A Green's tensor approach to the modeling of nanostructure replication and characterization

Michael Paulus and Olivier J. F. Martin

Electromagnetic Fields and Microwave Electronics Laboratory, Swiss Federal Institute of Technology, Zurich, Switzerland

[1]   We use the Green's tensor technique to study the optical processes taking place in configurations typically used for the replication and characterization of nanostructures. For the replication process we investigate light-coupling masks for optical contact lithography and for the characterization process the mode scattered by a defect or a short grating in a planar waveguide. Both configurations consist of structures embedded in a stratified background composed of a stack of material layers with different permittivities. We perform calculations for two-dimensional and three-dimensional structures and compare their optical behavior. Our results show that the additional material interfaces in three-dimensional systems can lead to significantly different field distributions and must be taken into account for a complete understanding of the electromagnetic properties of the systems.   INDEX TERMS: 0689 Electromagnetics: Wave propagation (4275); 0649 Electromagnetics: Optics; 0644 Electromagnetics: Numerical methods; 0669 Electromagnetics: Scattering and diffraction; 0624 Electromagnetics: Guided waves; KEYWORDS: scattering calculations, stratified media, light propagation, integrated optics, waveguides, optical lithography

1. Introduction

[2] Currently, feature sizes in integrated structures are being pushed down toward the 100 nm limit. Such small structures are not only required by the microelectronic industry [*Semiconductor Industry Association*, 2001], but also for integration in optoelectronics [*Hunsperger*, 1991]. Because these structures are smaller than the wavelength of light, it is a challenge to replicate them in an optical lithography process, as well as to understand their optical response with a standard characterization technique. Both processes rely equally on the interaction of light with subwavelength structures which are often embedded in a planar stratified medium consisting of several layers with different permittivities. Structured masks for optical contact lithography [*Cullmann*, 1985] and ridges on a multilayered waveguide [*März*, 1994] are only two examples of such systems with dielectric or metallic elements distributed in a layered background. Other examples stem from diffractive optics [*Schnabel et al.*, 1999], wafer inspection [*Sung et al.*, 1999], or bio-optics

[*Kahl and Voges*, 2000]. The accurate computation of light scattering in these structures is consequently very important for the design and optimization of specific components.

[3] Recently we presented a general technique for light propagation and scattering in structures formed by a stratified background with embedded scatterers [*Paulus et al.*, 2000; *Paulus and Martin*, 2001a, 2001b]. The scatterers can be two-dimensional (2-D), extending infinitely in one direction, or three-dimensional (3-D), with finite extension in all three directions. This approach is based on the Green's tensor associated with the stratified background and provides a rigorous solution of the vectorial wave equation with the boundary conditions given at the different material interfaces.

[4] In the present paper we apply our approach to the study of two exemplary configurations representing the replication and the characterization processes of nanostructures: Light-coupling masks (LCMs) for optical contact lithography and mode scattering by a defect in a planar waveguide. Our objective is to illustrate, from a modeling point of view, the similarities between these two classes of configurations.

[5] LCMs are siloxane polymer masks which have proven to be an efficient alternative for high-resolution sub-wavelength lithography [*Schmid et al.*, 1998a,
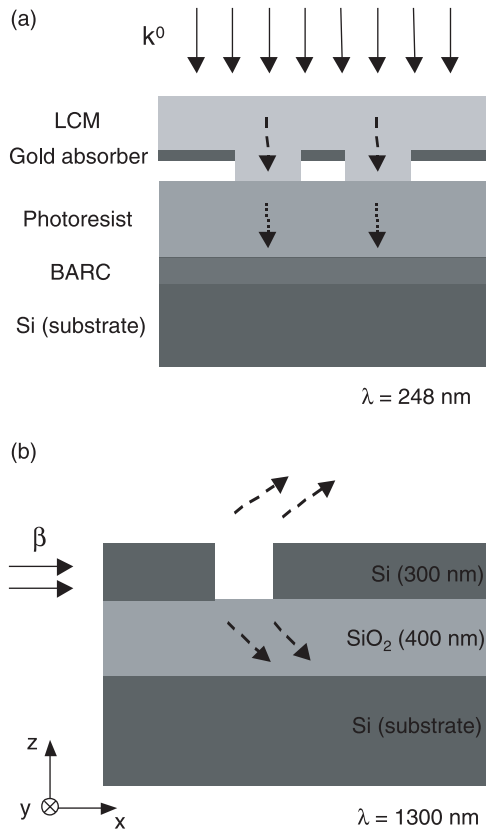
Figure 1. Cross-sectional view of the structures under study. (a) The stratified background of an LCM consists of the substrate, a bottom antireflection coating (BARC), the photoresist, an air gap, an absorbing metal layer and the mask backplane. The structure is illuminated from the top by a plane wave with wave vector $\mathbf{k}^0$. (b) The SOI waveguide consists of a Si and a SiO_2 layer on top of a Si substrate. The structure is illuminated by a mode with propagation constant β.

1998b]. The structures to be written in the photoresist are defined as protrusions on the mask. Being in contact with the photoresist, these protrusions guide and focus the light into the resist layer (Figure 1a). To increase the contrast, a thin gold layer is deposited at the noncontacting parts of the mask. Using a 248 nm illumination wavelength, LCMs allow the definition of structures in the sub-100 nm range.

[6] As an example from integrated optics we consider a silicon-on-insulator (SOI) planar waveguide with a defect formed by a rectangular notch etched from the top into the waveguide (Figure 1b). When a mode propagates in the waveguide and scatters on the defect, light is coupled out of the guiding layer and radiated into

the air and/or toward the substrate [*Orobtchouk et al.*, 2000].

[7] In section 2 we briefly describe our numerical approach and in section 3 we show results of simulations for the two configurations: LCMs are discussed in section 3.1 and waveguide mode scattering is investigated in section 3.2. In particular, we emphasize the different effects related to 2-D or 3-D scattering elements. Finally, we summarize our work in section 4.

2. Model

[8] The two systems under study, LCM and planar waveguide, are shown in Figure 1. Both structures consist of a stratified background composed of L layers with relative permittivity ε_l, $l = 1, \ldots, L$, and embedded scatterers with relative permittivity $\varepsilon(\mathbf{r})$. These scatterers correspond to the light guiding protrusions in the LCM and to the defects in the waveguide. The scatterers can be three-dimensional (3-D) with finite extension in all three directions or two-dimensional (2-D) extending infinitely in y direction. When such a system is illuminated with an incident electric field $\mathbf{E}^0(\mathbf{r})$ propagating in the stratified background, the total field $\mathbf{E}(\mathbf{r})$ is given as a solution of
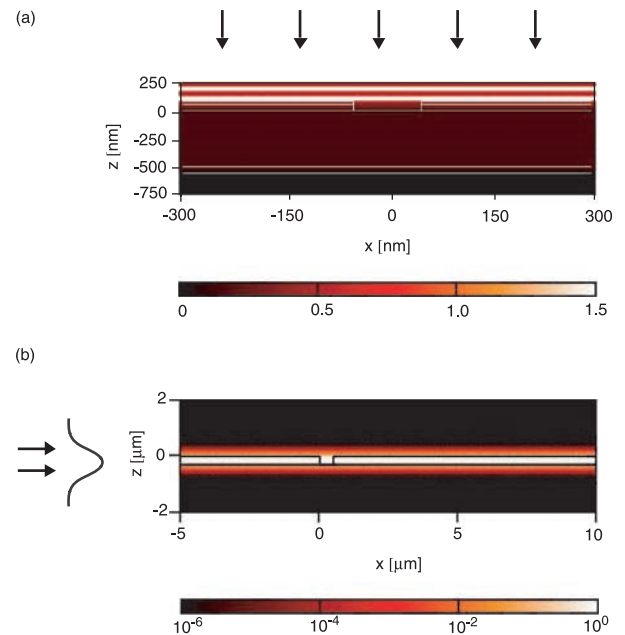

Figure 2. Different types of incident electric fields are possible for a given stratified background. In our simulations, we use (a) for the LCM a normally incident plane wave and (b) for the waveguide a guided mode. For clarity the entire structures including the scatterers are sketched.
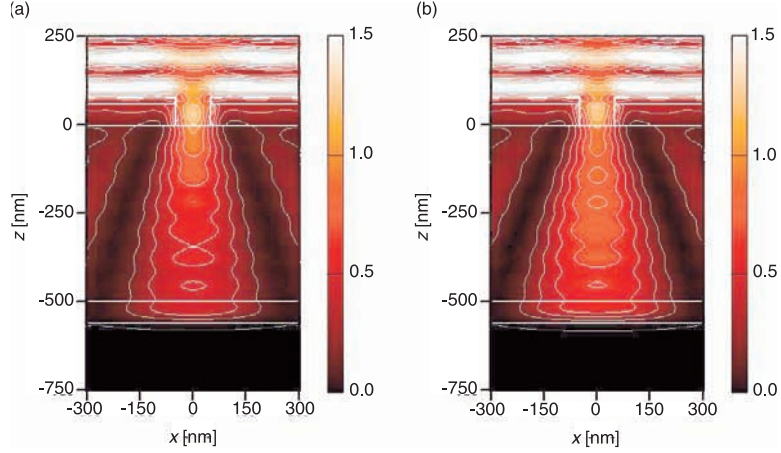
Figure 3. Electric field intensity distribution in an LCM structure comprising (a) a 2-D line (100 nm) and (b) a 3-D linelet (100 × 400 nm^2) at a wavelength λ = 248 nm. Cross-sectional view through the center of the structure (*xz* plane, *y* = 0). The color coding of the intensity is supported by isointensity lines representing increments of 10%.

the vectorial wave equation by the electric field integral equation (EFIE) [*Tai*, 1994]:

$$\mathbf{E}(\mathbf{r}) = \mathbf{E}^0(\mathbf{r}) + \int_V d\mathbf{r}' \mathbf{G}(\mathbf{r}, \mathbf{r}') \cdot k_0^2 \Delta\varepsilon(\mathbf{r}')\mathbf{E}(\mathbf{r}'), \quad (1)$$

where $\mathbf{G}(\mathbf{r}, \mathbf{r}')$ is the Green's tensor associated with the stratified background, $k_0^2 = \omega^2\varepsilon_0\mu_0$ the vacuum wave number and $\Delta\varepsilon(\mathbf{r})$ the dielectric contrast:

$$\Delta\varepsilon(\mathbf{r}) = \varepsilon(\mathbf{r}) - \varepsilon_\kappa, \quad \mathbf{r} \in \text{layer } \kappa. \quad (2)$$

The integration in (1) runs over the scatterers' section (2-D) or volume (3-D) V and can be evaluated numerically for example on a rectangular grid [*Martin and Piller*, 1998] or with tetrahedral finite elements [*Kottmann and Martin*, 2000]. It is important to note that the scatterers do not have to be embedded inside one background layer but can extend over several layers (the mask protrusions in Figure 1a cover both the metal layer and the air gap).

[9] The incident field $\mathbf{E}^0(\mathbf{r})$ must be a solution of the vectorial wave equation in the bare stratified background. Since this solution is not unique, different types of excitations are possible for a given material system. Figure 2 shows the incident fields used for the structures under study: The LCM is illuminated from the top by a plane wave with circular polarization (Figure 2a), and the waveguide is fed with a guided mode propagating inside the structure (Figure 2b). A further choice for $\mathbf{E}^0(\mathbf{r})$ could be for example a dipolar source embedded in the system or a surface plasmon propagating along the surface of a metallic layer.

[10] Since the integration in (1) runs only over the scatterers' volume, the discretization is also limited to the

scatterers, the stratified background being accounted for by the Green's tensor. More precisely, we only have to discretize the light guiding protrusions for the LCM simulation and the notch defects for the waveguide simulations. A further advantage is that the boundary conditions at the edges of the computation window as well as at the different material interfaces are perfectly and automatically fulfilled. They are already included in the Green's tensor and do not require any special treatment to avoid unphysical reflections as is the case with many other computational approaches [*Bérenger*, 1999].

[11] Whereas $\mathbf{G}(\mathbf{r}, \mathbf{r}')$ for an infinite homogeneous background can be expressed analytically, this is not possible when the background is stratified. However, in that case a numerical solution for $\mathbf{G}(\mathbf{r}, \mathbf{r}')$ based on Sommerfeld type integrals can be found. This quadrature is intricate because it involves several poles and branch cuts associated with the different electromagnetic modes that can be excited in the stratified background [*Chew*, 1995]. We recently developed an efficient computation technique for the evaluation of the Green's tensor in a stratified medium with 2-D or 3-D scatterers and refer the reader to *Paulus et al.* [2000] and *Paulus and Martin* [2001a, 2001b], where this technique is discussed in detail.

3. Numerical Results

3.1. Light-Coupling Masks

[12] For our study of LCMs we consider an isolated line with a width d = 100 nm as feature to be replicated. This line extends either infinitely in the *y* direction or is a

short line with length $4d$, a so-called "linelet." In the first case, a 2-D model is appropriate, whereas the latter case requires a fully 3-D treatment. The results presented here refer to a circularly polarized plane wave illumination normal to the mask surface, with a vacuum wavelength $\lambda = 248$ nm (the intensity of the incident field is normalized to unity). The relative permittivities are $\varepsilon = 2.25$ for the polymer mask background, $\varepsilon = 2.5$ for the photoresist, $\varepsilon = -0.9 + i4.3$ for gold, and $\varepsilon = -9 + i11$ for the silicon substrate [*Optical Society of America*, 1995]. The total height of the protrusion is 80 nm and the thickness of the gold absorber is 20 nm. To reduce the otherwise disturbing interference pattern due to reflections from the Si substrate, a 60 nm-thick bottom antireflection coating (BARC, $\varepsilon = 1.98 + i1.23$) is deposited on top of the substrate [*Macleod*, 1986]. The effect of the BARC for the incident plane wave illumination can be observed in Figure 2a, where the stationary wave in the resist layer is completely suppressed.

[13] The determinant parameter to characterize a given exposure is the electric field intensity $I = \mathbf{E} \cdot \mathbf{E}^*$ in the photoresist. Figure 3 shows cross-sectional views of the intensity distributions for the 2-D line and the 3-D linelet. Let us first mention that in both cases, in spite of the BARC, a weak stationary wave can be observed in the resist layer: The BARC is only optimal for a plane wave with a specific angle of incidence. The field guided through the protrusion into the photoresist, however, is not anymore a simple plane wave so that a weak interference pattern cannot be avoided.

[14] The overall intensity distributions for the 2-D and 3-D structures are quite similar. A closer look to the isointensity lines shows however that the intensity transmitted through the protrusion is larger for the 3-D linelet than for the 2-D line. For a more quantitative comparison we report in Figure 4a line cuts of the intensity in x direction at different depths in the photoresist, $z = -10$ nm, $z = -100$ nm, and $z = -200$ nm. Directly below the mask, at $z = -10$ nm, the two profiles are qualitatively similar with the maximal intensity being larger for the 2-D line. At $z = -100$ nm the profiles are nearly identical, but now the maximal intensity is slightly larger for the 3-D linelet. This situation changes at $z = -200$ nm, where the 3-D linelet shows a larger intensity and a broader field distribution. Note that for the 2-D line the relative intensity at the corners of the targeted structure is $I \approx 0.55$ at all three depths, providing steep edges of the developed photoresist. For the 3-D linelet the targeted structure is defined by the $I \approx 0.55$ isointensity line at $z = -10$ nm and $z = -100$ nm, but by $I \approx 0.7$ at $z = -200$ nm, leading to a broadening of the replicated structure in the photoresist depth. This confirms our observation from Figure 3: The mask protrusion's finite length in y direction increases the transmission as the additional material interfaces at the protrusion's endings
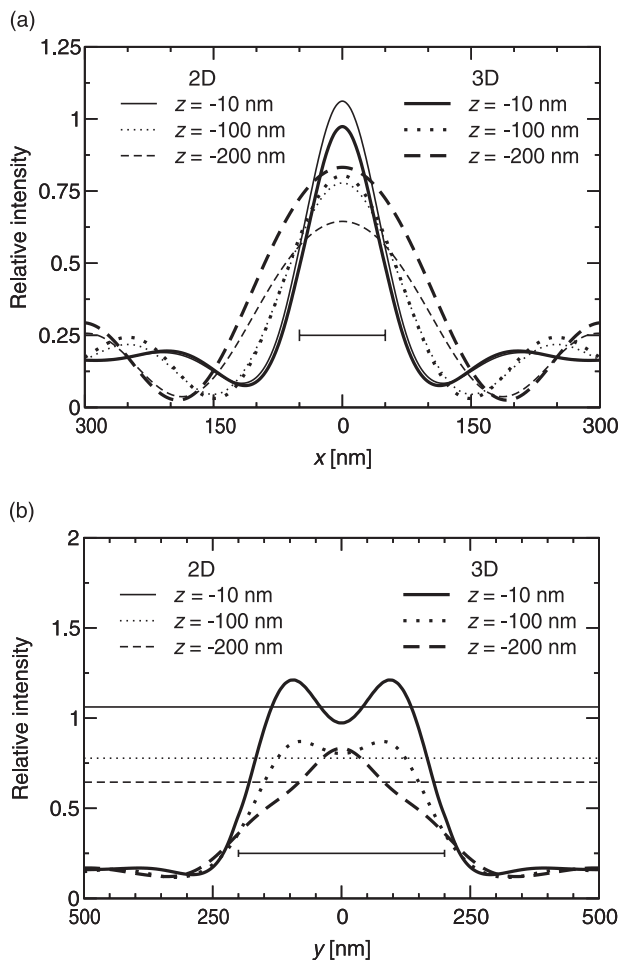
(a)

(b)

Figure 4. Intensity distributions at different depths in the photoresist, $z = -10$ nm, $z = -100$ nm, and $z = -200$ nm, for the 2-D line (thin) and the 3-D linelet (thick). Line cuts computed (a) along the x direction at $y = 0$ and (b) along the y direction at $x = 0$. The bar represents in Figure 4a the original line width and in Figure 4b the length of the original 3-D linelet.

augment the light throughput into the resist layer. Let us mention that this behavior is independent of the incident field polarization and can also be observed when $\mathbf{E}^0(\mathbf{r})$ is linearly polarized in x or in y direction (not shown).

[15] The influence of the linelet's finite length is of course much more pronounced in y direction, where, in contrast to the translation invariant 2-D structure, the transmitted light is confined by the additional material interfaces. Figure 4b shows line cuts through the intensity distributions in y direction at the same depths used previously. The profiles generated by the 2-D line are simply constant with the intensity values given in Figure
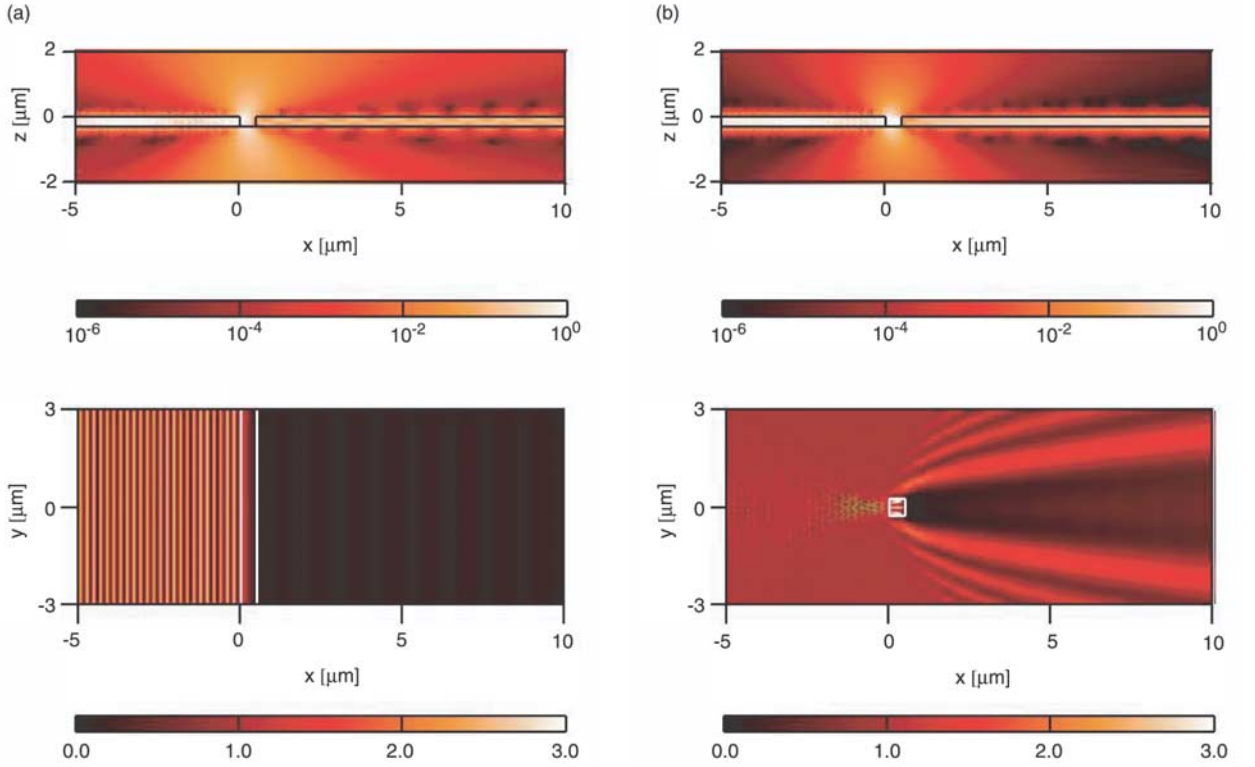
Figure 5. Electric field intensity distribution for the SOI waveguide structure with (a) a 2-D (500 nm × 300 nm^2) and (b) a 3-D (500 × 500 × 300 nm^3) notch. A TE$_0$ mode at a wavelength $\lambda = 1300$ nm propagating in $+x$ direction is used as illumination. The top row shows cross-sectional views through the center of the structure (xz plane, $y = 0$), the bottom row shows top views in the upper Si layer (xy plane, $z = -150$ nm).

4a at $x = 0$. For the 3-D linelet, however, we observe important intensity variations. Close to the mask at $z = -10$ nm, in the near field of the aperture, the intensity distribution is determined by a resonance in the linelet with two maxima. Less pronounced, this resonance is still visible at $z = -100$ nm. At $z = -200$ nm the two maxima merge into one single maximum. In practice, however, the photoresist is developed down to a certain intensity threshold and the intensity distribution above this threshold becomes irrelevant.

[16] For $y \approx \pm220$ nm all three line cuts cross with a relative intensity $I \approx 0.3$. At this point, steep edges provide a reliable replication of the linelet, but one must realize that the reproduced structure is $\approx10\%$ longer than the original linelet.

[17] Note that the line cuts in Figure 4a are computed in the $y = 0$ plane. From Figure 4b we learn that this plane corresponds to the minimum with respect to the y direction for $z = -10$ nm and $z = -100$ nm, but to the maximum for $z = -200$ nm. Further, the 3-D value at $x = y = 0$ is smaller than the corresponding 2-D value for $z = $

-10 nm, but larger for $z = -100$ nm and $z = -200$ nm, in agreement with the results obtained from Figure 4a.

3.2. Scattering in Planar Waveguides

[18] Let us now consider the SOI waveguide shown in Figure 1b with a 2-D or 3-D rectangular notch etched from the top into the upper Si layer. The notch extends 500 nm in x direction and, in the 3-D case, also 500 nm in y direction. The relative permittivities at the considered wavelength $\lambda = 1300$ nm are $\varepsilon = 12.3$ for the Si and $\varepsilon = 2.1$ for the SiO$_2$ [*Optical Society of America*, 1995].

[19] Figure 5 shows electric field intensity distributions $I = \mathbf{E} \cdot \mathbf{E}^*$ when the waveguide is illuminated with a TE$_0$ mode (electric field polarized in y direction) propagating in $+x$ direction (the mode is normalized so that the maximum electric field intensity is unity). In the cross-sectional view (Figure 5, top row) the field distributions for the 2-D and the 3-D geometries are quite similar, the 2-D notch leading to more light coupled out of the waveguide. In the top view (Figure 5, bottom row) the differ-
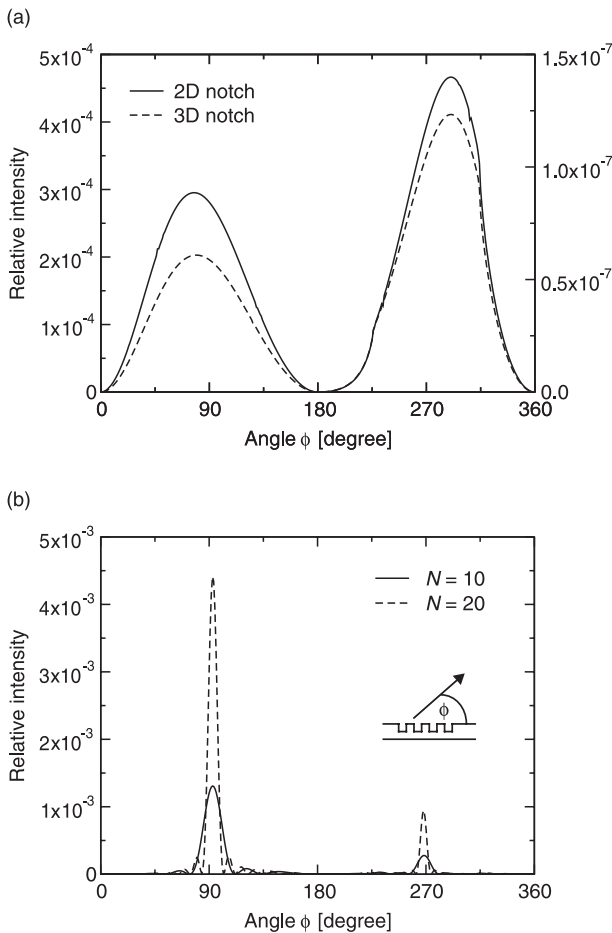
(a)

(b)

Figure 6. Angular distribution of the scattered far field intensity for the SOI waveguide with (a) one single 2-D (left scale) or 3-D (right scale) notch and (b) a short grating consisting of $N = 10$ or $N = 20$ 2-D lines. The inset in (b) shows the definition of the angle ϕ. The TE_0 mode is used as illumination.

ences between 2-D and 3-D become much more obvious. The interaction of the incoming field and the field scattered by the 2-D notch leads in backward direction to a stationary wave parallel to the y axis, the translation axis of the system (Figure 5a, bottom row). In forward direction the transmitted mode propagates further with decreased intensity. A much more complex interference pattern is created by the 3-D notch (Figure 5b, bottom row). In backward direction the stationary wave now forms a system of fringes and in forward direction we recognize the diffraction pattern of the rectangular notch. We already discussed this behavior for the replication of 3-D features with LCMs in Figure 4: Whereas a 2-D structure leads to a homogeneous field distribution in y

direction, the field of the 3-D structure has significant variations in this direction.

[20] Let us now study the effect of the defects on the signal measured far away from the structure. Figure 6a shows the angular distribution of the radiated far field intensity for the 2-D and the 3-D notch. The radiation pattern are qualitatively very similar, but, as we already observed in Figure 5, the perturbation of the mode is much stronger with a 2-D notch interrupting the mode completely. The radiation lobes both in the air and the substrate are rather broad, with maxima at $\phi = 78°$ and $\phi = 290°$ corresponding to a radiation in forward direction. More energy is coupled into the substrate than into the air. This characteristic radiation pattern changes, when additional defects are deposited on the waveguide. Figure 6b reports the far field intensity for 10 and 20 2-D scattering elements, forming two short gratings with a periodicity $d = 400$ nm and a 0.5 filling factor. The lobes become more narrow with an increasing number of elements, creating two well defined beams of outcoupled light at $\phi = 93°$ into the air and at $\phi = 268°$ toward the substrate. The gratings radiate into small angular ranges approximately normal to the waveguide surface. At the same time, the maximum outcoupled intensity increases with the number of elements. It is remarkable that the radiation is now strongest into the air with the maximum intensity being approximately five times larger than that toward the substrate. This behavior is significantly different from that of a single notch, where the scattering into the substrate was dominant (compare Figures 6a and 6b).

4. Summary

[21] Configurations used for the replication and those used for the characterization of nanostructures are often similarly formed by elements embedded in a stratified background. In both systems, the scattering and propagation of light determines the total electric field distributions; hence it determines the experimentally measured quantities. In this paper we applied the Green's tensor technique to investigate two representative configurations: light-coupling masks for optical contact lithography and mode scattering in a planar SOI waveguide. The Green's tensor technique is very well suited for this type of structures because the optical processes in the stratified background are accurately described by the Green's tensor. This technique can handle both 2-D and 3-D systems, which allowed us to compare their corresponding scattering properties. Although 2-D calculations are generally less computing intensive, our results indicate that a 2-D model is only valid when the electromagnetic field is so well localized that edge effects become negligible. For many practical configurations these edge effects must be taken into account for a complete and correct description of the optical processes.

References

Bérenger, J.-P., Evanescent waves in PML's: Origin of the numerical reflections in wave-structure interaction problems, *IEEE Trans. Antennas Propag.*, *47*, 1497–1503, 1999.

Chew, W. C., *Waves and Fields in Inhomogeneous Media*, IEEE Press, New York, 1995.

Cullmann, E., Excimer laser applications in contact printing, *Semicond. Int.*, *8*, 332–334, 1985.

Hunsperger, R. G., *Integrated Optics: Theory and Technology*, 3rd ed., Springer-Verlag, New York, 1991.

Kahl, M., and E. Voges, Analysis of plasmon resonance and surface-enhanced Raman scattering on periodic silver structures, *Phys. Rev. B*, *61*, 14,078–14,088, 2000.

Kottmann, J. P., and O. J. F. Martin, Accurate solution of the volume integral equation for high permittivity scatterers, *IEEE Trans. Antennas Propag.*, *48*, 1719–1726, 2000.

Macleod, H. A., *Thin-Film Optical Filters*, 2nd ed., Adam Hilger, Bristol, UK, 1986.

Martin, O. J. F., and N. B. Piller, Electromagnetic scattering in polarizable backgrounds, *Phys. Rev. E*, *58*, 3909–3915, 1998.

März, R., *Integrated Optics Design and Modeling*, Artech House, Norwell, Mass., 1994.

Optical Society of America, *Handbook of Optics*, vol. II, 2nd ed., McGraw-Hill, New York, 1995.

Orobtchouk, R., A. Layadi, H. Gualous, D. Pascal, A. Koster, and S. Laval, High-efficiency light coupling in a submicrometric silicon-on-insulator waveguide, *Appl. Opt.*, *39*, 5773–5777, 2000.

Paulus, M., and O. J. F. Martin, Light propagation and scattering in stratified media: A Green's tensor approach, *J. Opt. Soc. Am. A*, *18*, 854–861, 2001a.

Paulus, M., and O. J. F. Martin, Green's tensor technique for scattering in two-dimensional stratified media, *Phys. Rev. E*, *63*, doi:10.1103/PhysRevE.63.066615, 2001b.

Paulus, M., P. Gay-Balmaz, and O. J. F. Martin, Accurate and efficient computation of the Green's tensor for stratified media, *Phys. Rev. E*, *62*, 5797–5807, 2000.

Schmid, H., H. Biebuyck, B. Michel, and O. J. F. Martin, Light-coupling masks for lensless, sub-wavelength optical lithography, *Appl. Phys. Lett.*, *72*, 2379–2381, 1998a.

Schmid, H., H. Biebuyck, B. Michel, O. J. F. Martin, and N. B. Piller, Light-coupling masks: An alternative, lensless approach to high-resolution optical contact lithography, *J. Vac. Sci. Technol. B*, *16*, 3422–3425, 1998b.

Schnabel, B., E. B. Kley, and F. Wyrowski, Study on polarizing visible light by subwavelength-period metal-stripe gratings, *Opt. Eng.*, *38*, 220–226, 1999.

Semiconductor Industry Association, *International Technology Roadmap for Semiconductors: 2001 Edition*, Semicond. Ind. Assoc., San Jose, Calif., 2001. (Available at http://public. itrs.net.).

Sung, L. P., G. W. Mulholland, and T. A. Germer, Polarized light-scattering measurements of dielectric spheres upon a silicon surface, *Opt. Lett.*, *24*, 866–868, 1999.

Tai, C.-T., *Dyadic Green Function in Electromagnetic Theory*, IEEE Press, New York, 1994.

O. J. F. Martin and M. Paulus, Electromagnetic Fields and Microwave Electronics Laboratory, Swiss Federal Institute of Technology, ETH-Zentrum ETZ, CH-8092 Zurich, Switzerland. (martin@ifh.ee.ethz.ch; paulus@ifh.ee.ethz.ch)